J. Ocean Univ. China (Oceanic and Coastal Sea Research)
https://doi.org/10.1007/s11802-019-3983-6
ISSN 1672-5182, 2019 18 (5): 1105-1114
http://www.ouc.edu.cn/xbywb/
E-mail:xbywb@ouc.edu.cn

Moho Structure of the Southwest Sub-Basin, South China Sea, from a Multichannel Seismic Reflection Profile NH973-1

ZHANG Jinchang[1)], CHEN Jie[2), 3), *], and HUANG Yanming[4)]

1) *CAS Key Laboratory of Ocean and Marginal Sea Geology*, *South China Sea Institute of Oceanology*, *Chinese Academy of Sciences*, *Guangzhou* 510301, *China*
2) *Fourth Institute of Oceanography*, *Ministry of Natural Resources*, *Beihai* 536007, *China*
3) *South China Sea Institute of Planning and Environmental Research*, *Ministry of Natural Resources*, *Guangzhou* 510310, *China*
4) *Key Laboratory of Exploration Technologies for Oil and Gas Resources*, *Ministry of Education*, *Yangtze University*, *Wuhan* 430100, *China*

(Received August 19, 2018; revised October 8, 2018; accepted January 29, 2019)

Abstract Moho structure provides important clues for understanding crustal structure, isostatic state and magmatic flux from mantle to surface. Across-basin Moho structure of the South China Sea (SCS) is important for understanding crustal evolution mechanisms of both continental break-up and seafloor spreading processes. Southwest Sub-basin (SWSB) opened up the latest and has the closest continental margins, making it the best to study the across-basin structure. Multichannel seismic (MCS) reflection data of line NH973-1 that crosses SWSB in NW-SE direction were reprocessed in order to image Moho structure. In MCS data, Moho reflectors are observed in places, which were not revealed in prior researches. The Moho generally shows symmetric structure on both sides of the central rift valley (CRV) and with variations in crustal thickness. Around CRV, the Moho is 2 seconds depth in two-way travel time (TWTT) beneath the igneous basement, which corresponds to 7 km depth, indicating normal oceanic crustal accretion during the ending of seafloor spreading. Close to the continent-ocean boundary (COB), the Moho becomes shallow to 1 second depth in TWTT (3.5 km), implying strong crustal thinning towards the continent, probably because of poor magma supply at the beginning of seafloor spreading. At south COB, the Moho depth under the crust almost reaches zero, which could be explained as a result of exhumed mantle. In addition, two low-angle, deep-penetrating normal faults are observed at south COB. The faults cut across the Moho into the upper mantle, which may be attributed to lithospheric hyper-stretching at COB during continental break-up.

Key words Moho structure; multichannel seismic reflection; crustal structure; South China Sea; oceanic basin; continent-ocean boundary

1 Introduction

The Mohorovičić discontinuity (also known as Moho) is commonly recognized as the boundary between the crust and the mantle. The structure of the Moho is important for studies of crustal thickness, magmatic flux from mantle to crust, and plate tectonics (Steinhart, 1967). The Moho, in petrology, is hypothesized as the interface between non-peridotitic crustal rocks (with gabbro composition) and olivine-dominated mantle rocks (with peridotite composition) (Nedimovic *et al*., 2005). Nevertheless, this interface is hidden deep within the Earth and has not yet been directly sampled, so the petrologic nature of the Moho is still a mystery. Although the Moho depths are usually predicted by gravity anomaly and isostatic compensation model based on surface features in topography (*e.g*., Sandwell and MacKenzie, 1989; Sandwell and Smith, 1997; Kearey *et al*., 2009), deep-penetrating seismic sounding is the only direct method to observe Moho geometry and measure crustal structure (*e.g*., Holbrook *et al*., 1992; Mutter and Carton, 2013; Zhang *et al*., 2016b).

In seismic measurement, the Moho is defined by a change of elastic parameters (velocity and density). When the Moho is >10 km below the seafloor, its structural information comes primarily from wide-angle seismic refraction. The Moho marks a first-order velocity discontinuity from crustal values of $<7.2\,\mathrm{km\,s^{-1}}$ to mantle values of $>8.0\,\mathrm{km\,s^{-1}}$ (Rohr *et al*., 1988; Holbrook *et al*., 1992). Refraction data generate a velocity-depth section using seismic wave travel curves and ray tracing models (*e.g*., Korenaga and Sager, 2012). This technique, however, just produces a smoothed view of Moho structure. In contrast, near-vertical incidence multichannel seismic (MCS) re-

* Corresponding author. E-mail: carrie_ocean@sohu.com

flection profiling is a better candidate to image the Moho and measure its geometry. In particular, the Moho can be well observed when it is shallow (<10 km below the seafloor), such as underneath normal oceanic crusts accreted by seafloor spreading (*e.g.*, Kent *et al.*, 1994; Mutter and Carton, 2013; Aghaei *et al.*, 2014; Zhang *et al.*, 2016b).

South China Sea (SCS), located in the west Pacific Ocean (Fig.1), is the largest marginal sea in low-latitude areas on Earth. Most scientists claim that the development of this oceanic basin initiated by continental break-up in late Cretaceous to early Paleogene (85–40 Myr) and followed by seafloor spreading in late Oligocene to middle Miocene (33–15 Myr) (Taylor and Hayes, 1980, 1983; Briais *et al.*, 1993; Hsu *et al.*, 2004; Barckhausen *et al.*, 2014; Li *et al.*, 2014).

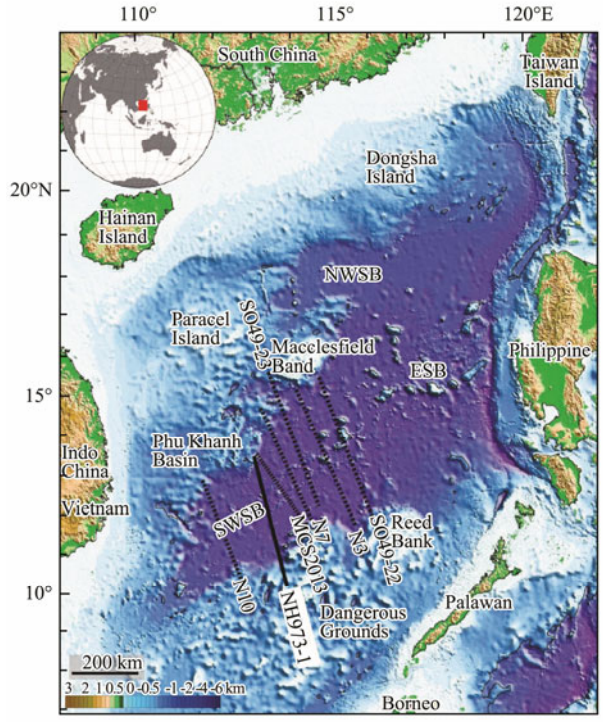

Fig.1 Southwest Sub-basin bathymetry map within SCS and nearby tectonic units. Background is satellite-predicted bathymetry from Smith and Sandwell (1997). Black solid and dash lines denote MCS reflection lines. SWSB, Southwest Sub-basin; ESB, East Sub-basin; NWSB, Northwest Sub-basin. Inset shows location of SCS in global scale.

The origin of SCS is under debate. One mechanism is the extrusion-based model, which suggests that SCS opened due to the extrusion of Indo-China relative to South China driven by the collision between India and Asia (*e.g.*, Briais *et al.*, 1993; Replumaz and Tapponnier, 2003). The other is the subduction-based model, which proposes that the opening of SCS resulted from slab pull when proto-South China subducted underneath Borneo (*e.g.*, Holloway, 1982; Hall, 2002; Hall *et al.*, 2008; Pubellier and Morley, 2014). These two end-member mechanisms are supported by some geophysical and geochemical data, but either is not fit with the other, so modified or hybrid models need to be developed in order to incorporate extra complexities (Cullen *et al.*, 2010). For example, the Hainan mantle plume causing additional lithospheric thinning is suggested as a required piece to the puzzle of SCS opening (Xia *et al.*, 2016).

Southwest Sub-basin (SWSB) is one of the three sub-basins in SCS, with a V-shape bounded by the Paracel Island, Macclesfield Bank, Vietnam continental margin, and Dangerous Grounds (Fig.1). SWSB is unique among all SCS sub-basins because it opened the latest and has the narrowest conjugate continental margins. Hence, it provides the best opportunity to run across-basin seismic lines to study structural footprints recorded at the continent-ocean boundary (COB) and in the oceanic basin, showing a continuous process from continental break-up to seafloor spreading. However, the seismic Moho structure is still poorly known because of the scarcity of modern, deep-penetrating seismic data (Lei and Ren, 2016; Lei *et al.*, 2018). This situation spurred several recent seismic surveys, including a representative joint refraction and reflection line, NH973-1, collected by *R/V Tan Bao* in 2009 (Fig.1). In this paper, we describe the Moho geometry of SWSB using reprocessed MCS reflection data of line NH973-1, determine crustal thickness across the basin, and discuss implications for how the basin was created by continental break-up and subsequent seafloor spreading. This study shows the crustal structure beneath SWSB with unprecedented details, providing new insights to the formation and evolution of SCS and marginal seas.

2 Prior Studies on Deep Crustal Structure of SWSB

2.1 COB and Rifted Margin

Although many passive continental margins in the world are volcanic rifted margins (Skogseid, 2001; Menzies *et al.*, 2002; Franke *et al.*, 2013), SCS appears to be a different case. Wide-angle seismic refraction data show 80 km wide crustal thinning over COB, characterized by crustal thickness decreasing from 20 km on the continental margin to 6 km in the oceanic basin (Lu *et al.*, 2011; Qiu *et al.*, 2011; Ruan *et al.*, 2011; Pichot *et al.*, 2013). This extensive crustal thinning, together with large detachment faults seen in MCS profiles (Hu *et al.*, 2009; Li, 2011; Zhao *et al.*, 2011; Franke *et al.*, 2011, 2013; Ding *et al.*, 2013, 2016), implies the non-volcanic type of passive margin classified as rifting driven by the forces of plate boundary with poor magmatic intrusions and extrusions (Geoffroy, 2005; Franke, 2013), such as Iberia-New-foundland margin (Boillot *et al.*, 1995; Manatschal and Bernoulli, 1999; Whitmarsh *et al.*, 2001; Hopper *et al.*, 2007; Reston, 2007; Tucholke and Sibuet, 2007; Peron-Pinvidic and Manatschal, 2009), NW Australian margin (Karner and Driscoll, 1999), and Brazil-Angola margin (Mohriak *et al.*, 1990; Contrucci *et al.*, 2004; Aslanian *et al.*, 2010; Contreras *et al.*, 2010). In addition, no evidence of seaward dipping reflectors, as well as little syn-rift magmatism (Yan *et al.*, 2006) supports this hypothesis of magma-poor margin. The SCS margin, however, has not shown extreme crustal stretch-

ing that may cause mantle exhumation along detachment faults at COB (*e.g.*, Iberia-Newfoundland margin, Peron-Pinvidic and Manatschal, 2009). Notably, to the northwest of SWSB, the Phu Khanh Basin shows evidence of hyper-stretching crust and possible exhumation of the mantle (Fig.1, Franke, 2013; Savva *et al.*, 2013). Regarding the adjacent location, SWSB is likely to undergo similar tectonic process. MCS data can therefore test this similarity by examining the detailed crustal structure of SWSB.

2.2 Oceanic Basin and Oceanic Crust

SWSB is proved to be an oceanic basin formed by seafloor spreading (Yao and Wang, 1983; Qiu *et al.*, 2011; Wu *et al.*, 2012b; Pichot *et al.*, 2013; Li *et al.*, 2014). Sonobouy, twin-ship refraction data reveal that the crust within SWSB is 7 km thick, similar to normal oceanic crust in other places (Yao and Wang, 1983). More recently, ocean bottom seismometer (OBS) data further show the Moho geometry and crustal thickness in the basin, giving nearly the same structural picture of normal oceanic crust (Qiu *et al.*, 2011; Wu *et al.*, 2012b; Pichot *et al.*, 2013). Nevertheless, in the oceanic basin, low density of receiving stations in seismic refraction exploration produces low resolution crustal images, and the smoothed Moho models hardly provide details about variations of crustal thickness across the basin. Modern, deep-penetrating MCS data can therefore have the potential to solve this problem, which helps further understand the crustal accretion of SWSB.

3 Data and Methods

Prior to the recent MCS surveys, there were two seismic lines acquired in 1987 across the eastern part of SWSB (SO49-22, SO49-23; Fig.1). Owing to small sound source and short receiving array used in data acquisition, these two profiles only show the sediment structure, but rarely display penetration below the igneous basement (Li *et al.*, 2012). Therefore, these data are not useful for examining the subbasement structure.

Modern, deep penetrating across-basin MCS reflection profiles were collected over the central part of SWSB from *R/V Tanbao* in 2004, 2009 and 2013 (N3, N7, N10, NH973-1, MCS2013; Fig.1). These profiles were acquired by an airgun source of 83.3 L and a receiving array of 480 channels. The seismic lines were run with a 50 m shot interval and a 12.5 m receiver interval. The reflection data had sampling rate of 2 ms and record length of 12 s (Figs.3–7 only show 10 s in depth because below 10 s the seismic singal is too noisy to identify reflectors). Due to data access limitation, we just had the MCS data of line NH973-1 for processing and interpretation, but it can serve as a representative of the MCS lines that cross SWSB.

Although few Moho reflectors were observed in the NH973-1 profile with standard processing, the data were reprocessed by constant velocity stacks (CVS) to improve the Moho imaging (Fig.2), instead of normal common depth point (CDP) stacks with a velocity-depth model based velocity analysis. CVS is a processing approach that uses a pre-determined constant velocity for the entire time domain to stack CDP traces. In MCS data, the Moho reflection is typically deep and weak in amplitude, so it is hard to obtain an optimal stacking velocity for the Moho by analyzing the semblance. We tested a range of plausible velocities (3000–5000 m s^{-1} with 50 m s^{-1} step length) in CVS to search for the value that provided the clearest image (3750 m s^{-1}). This stacking velocity corresponds to 8000 m s^{-1} interval velocity (using Dix Formula; Dix, 1955), which matches with the Moho velocity value in OBS refraction results of line NH973-1 (Qiu *et al.*, 2011). Hence, CVS has the advantage of simplicity and the ability of highlighting reflectivity of a particular horizon (here the Moho) when coherency or semblance does not work well because of low signal-noise ratio or lack of layered structures. Because CVS more or less results in the degradation of image quality for structures above the Moho, this method cannot be used as standard seismic reflection imaging for a complete section. However, the CVS technique is simple and practical to improve the visibility of the deep, isolated Moho reflectors in seismic sections (*e.g.*, Zhang *et al.*, 2016b).

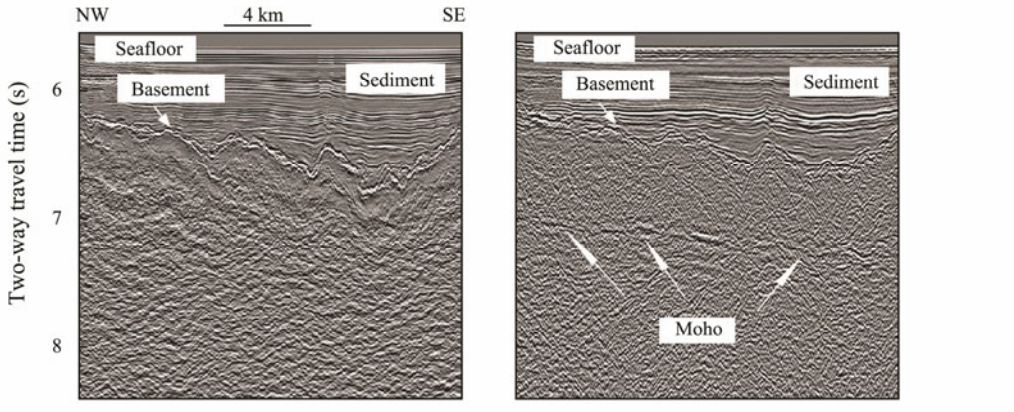

Fig.2 Moho imaging effect comparison between the normal CDP stack (left) and the constant velocity stack by using a stacking velocity of 3750 m s^{-1} (right). This selected portion from MCS reflection line NH973-1 is located close to the north COB of SWSB. Vertical exaggeration = 2:1. Location is shown in Fig.3.

For the Moho interpretation, this interface was correlated with the deepest visible reflector in MCS reflection profiles. Usually, the Moho is the only deep reflection in a MCS section, otherwise there is no such signals. Although no direct evidence verifies the nature of this reflector to be the Moho, no other plausible explanations are proposed either. What is more, interpretation of this reflection as Moho appears to be consistent with the results from OBS refraction data in the oceans (*e.g.*, Prada *et al.*, 2012; Zhang *et al.*, 2016b).

4 Results

4.1 Reflection Moho Characteristics

Across SWSB, reflection Moho is observed in many places (Fig.3), especially in the basin itself where the Moho is shallow beneath the seafloor and the crust is relatively thin. This characteristic is consistent with those in other basins in that reflection Moho is observable when the crust is <10 km thick (Kent *et al.*, 1994; Mutter and Carton, 2013; Aghaei *et al.*, 2014; Zhang *et al.*, 2016b). However, on the surrounding continental margins with much thicker crust (up to 20 km and more, Qiu *et al.*, 2011), reflection Moho is hardly seen, likely due to nearly complete seismic signal attenuation in such great Moho depth or noisy multiples masking.

Generally, the Moho reflection shows discontinuity in SWSB (Figs.4–7). Gaps occur between reflector segments, ranging a few to tens of kilometers. Shapes of reflector segments are basically flat but sometimes curved. Their amplitudes present variability in strong or weak strength. These segments can nevertheless be connected and traced through the basin, demonstrating the crustal structure in larger scale. This charateristic of discontinuous reflection Moho can be also seen over other ocean basins (Mutter and Carton, 2013). Possible causes for the Moho discontinuity include actual complex Moho structure varying from a sharp acoustic boundary to a broad transition zone, as well as imaging conditions affected by near-surface structure (Zhang *et al.*, 2016b). The latter infers that smooth, flat-layered upper crustal topography (*e.g.*, Fig.4, shot points (SP) 100–600) provides a good condition to observe Moho reflectors, but rough, complex-layered topography (*e.g.*, Fig.5, SP 2200–2600) might scatter the penetrating seismic energy, resulting in no signal return to the surface.

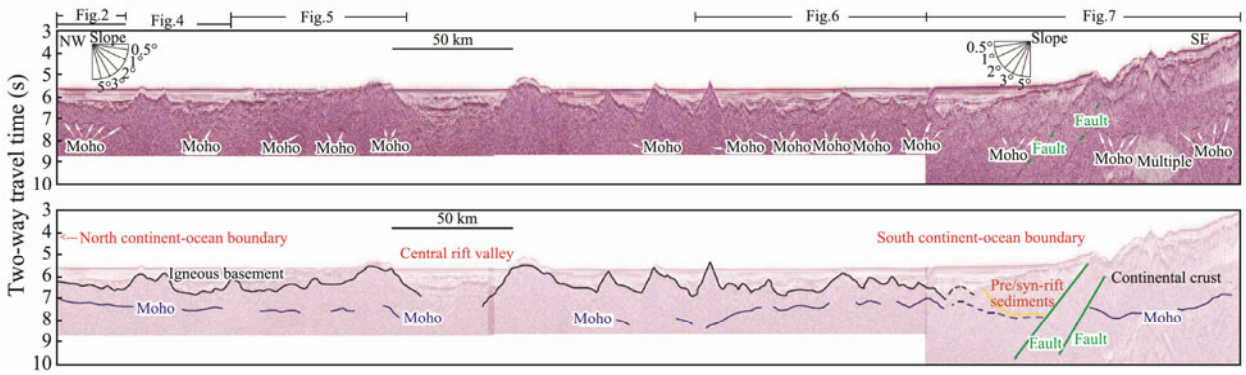

Fig.3 MCS reflection images and crustal structure across SWSB. Upper panel is the MCS reflection images of line NH973-1, in which Moho reflectors are displayed. Enlarged images of four segments from line NH973-1 are shown in Figs.4–7. Slope indicators are calculated by a crustal average velocity of 7000 m s^{-1}. Vertical exaggeration = 5:1. Lower panel shows the interpretation of crustal structure along the seismic line. Black lines represent the igneous basement. Layers above the basement are sediments. Blue lines show the Moho reflectors. Green lines denote two large crustal faults. Yellow line denotes the bottom of the pre/syn-rift sediments within the south COB, from Zhao *et al.* (2011), Ding *et al.* (2013), Song and Li (2015) and Wang *et al.* (2016). Line location is shown in Fig.1.

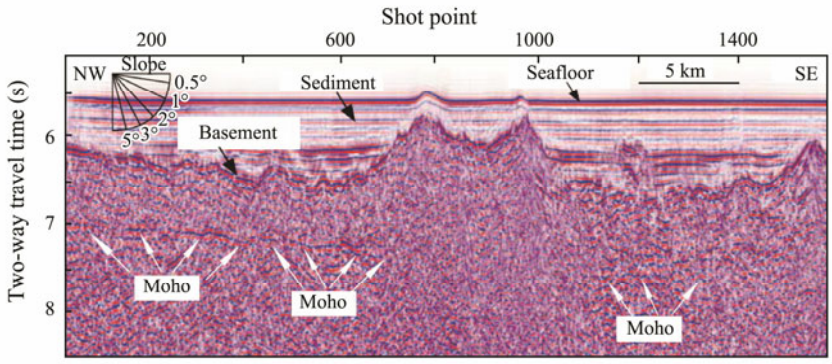

Fig.4 MCS reflection image displaying Moho reflectors from a segment of line NH973-1 close to the north COB of SWSB. Other plot conventions are the same as in Fig.3. Segment location is shown in Fig.3.

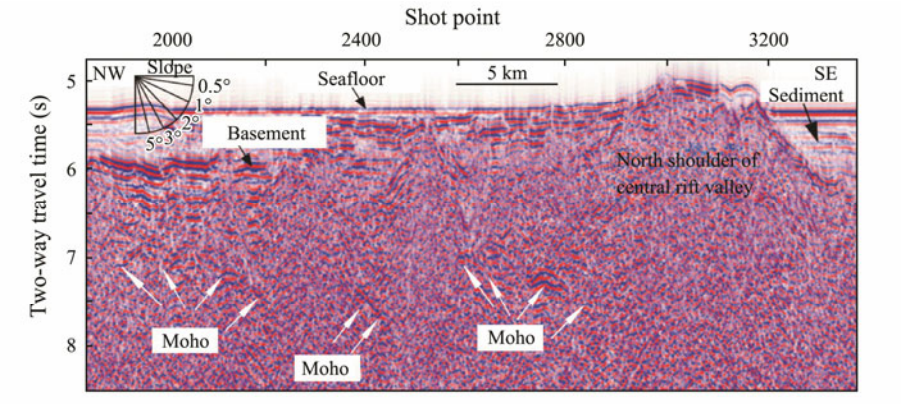

Fig.5 MCS reflection image displaying Moho reflectors from a segment of line NH973-1 to the north of CRV in the middle of SWSB. Other plot conventions are the same as in Fig.3. Segment location is shown in Fig.3.

4.2 Moho Reflectors Across SWSB

At the north margin of SWSB (close to north COB), clear and continuous Moho reflectors are observed underneath the seafloor (Fig.4), starting from a depth of 7 s in two-way travel time (TWTT), *i.e.*, 1 s TWTT beneath the igneous basement corresponding to 3.5 km in crustal thickness (assuming a crustal average velocity of 7000 m s^{-1}). The Moho reflectors dip towards the basin center with a gentle slope of 0.5°. A twin-peak basement high at SP 700–1000 interrupts the continuity of the Moho reflection. As mentioned above (Section 4.1), the Moho disappears herein probably due to rough upper topography scattering or seismic signal attenuation. Nonetheless, on the south of the basement high where the basement becomes smooth and flat, Moho reflectors are seen again and can be connected with the north ones. Farther to the south, the Moho runs into another basement high and gets truncated again.

Following the trend from the north margin of SWSB, the north flank of the central rift valley (CRV) shows similar Moho structure (Fig.5). Moho reflectors continue gently dipping towards the center of the basin, with a slightly increasing depth under the basement from 1.5 s TWTT (5 km thick crust) in the north to 2 s TWTT (7 km thick crust) in the south where close to CRV. Likewise, the Moho is truncated by rough basement topography, *e.g.*, two basement highs (SP 2300 and 2500) and the north shoulder of CRV (SP 3100).

On the south flank of CRV, the Moho reflectors appear to be symmetric compared to the north (Fig.6). The Moho occurs at 2 s TWTT (7 km crustal thickness) beneath the basement to the south shoulder of CRV, then becomes shallower towards south, reaching <1 s TWTT (<3.5 km crustal thickness) near the south COB. The basement is fairly rough in this area as many faulted blocks are seen, yielding highly discontinuity in the Moho reflection.

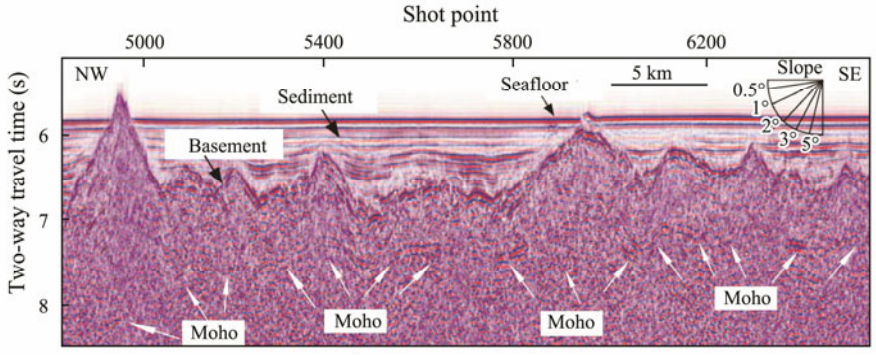

Fig.6 MCS reflection image displaying Moho reflectors from a segment of line NH973-1 to the south of CRV in the middle of SWSB. Other plot conventions are the same as in Fig.3. Segment location is shown in Fig.3.

At the south COB (Fig.7), the shallow Moho nearly pinches out underneath the pre/syn-rift sediments suggested by Zhao *et al*. (2011), Ding *et al*. (2013), Song and Li (2015) and Wang *et al*. (2016), implying little oceanic crust existence and likely upper mantle exhumation. Two normal faults are observed nearby. They are almost parallel to each other and both dip towards the ocean basin with a low angle of 2°. The extension of the two faults cuts through the whole crust as well as the Moho and goes into the upper mantle. These two deep reaching faults, together with nearly zero crust occurring at the COB, imply hyper-stretching in the lithosphere during continental break-up. Meanwhile, the complex crustal structure resulting from the two faults leads to disappearance of the Moho in the faulting zone. However, farther to the south and onto the continental margin, the Moho appears at a depth of 2 s

TWTT beneath the continental crust. Subsequently, the continental crustal thickness increases towards south.

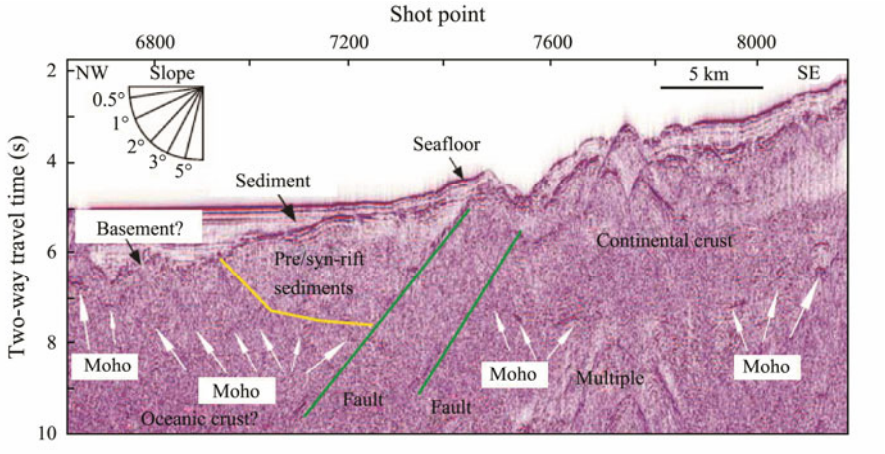

Fig.7 MCS reflection image displaying Moho reflectors from a segment of line NH973-1 at the south COB of SWSB. Yellow line denotes the bottom of the pre/syn-rift sediments (Zhao *et al*., 2011; Ding *et al*., 2013; Song and Li, 2015; Wang *et al*., 2016). Green lines represent the faults. Other plot conventions are the same as in Fig.3. Segment location is shown in Fig.3.

5 Discussion

5.1 Crustal Structure and Tectonic Evolution of SWSB

Either old refraction data from sonobouy (Yao and Wang, 1983) or recent wide-angle data from OBS (Qiu *et al*., 2011; Wu *et al*., 2012b; Pichot *et al*., 2013; Yu *et al*., 2017) did not show detailed crustal structure of SWSB owing to too much interpolation and smoothing application. The former are acquired by an out-of-date technique, whereas the latter are collected with sparse receiving stations. Hence, the fine crustal structure and variations of crustal thickness in SWSB are not revealed until our MCS study in this paper. As observed on the MCS reflection line NH973-1 across SWSB, the large-scale picture is the symmetric Moho structure to CRV (Fig.3). Around CRV, the Moho is 2 s TWTT depth below the igneous basement (7 km in crustal thickness), whereas becoming shallower towards COB. Remarkably, at south COB, there is probably no crust (*i.e*., mantle exhumation), and there are two low-angle dipping, normal faults penetrating deep into the mantle. Moreover, the continental crust thins towards the south COB.

The crustal structure observations provide insight to the tectonic evolution of SWSB (Fig.8). Hyper-stretching of the continental lithosphere, proved by the thinning continental crust towards the ocean basin and the two deep normal faults that we observed at the south COB, may give a chance for upper mantle to exhume to the surface. At the same time or soon after the continent breaks up into margins, poor magma outpours onto the exhumed mantle, generating very thin oceanic crust during the starting stage of seafloor spreading. With the progress of seafloor spreading, magma supply increases gradually with time and accretes progressively thicker crust. In the end, magma supply brings up to normal as other ocean basins, ceases with a normal oceanic crustal thickness of 7 km and leaves a CRV structure in the middle of the basin.

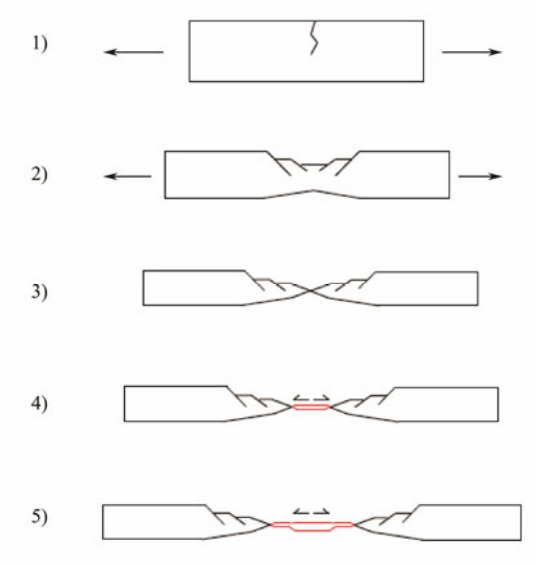

Fig.8 A model proposed to demonstrate the tectonic evolution of SWSB. Black plates represent continental lithosphere. Red plates denote oceanic crust. Black arrows show the plate moving directions. Tilted black lines on the surface of continental lithosphere are faults in the plate. Sketches are not to actual scale. Phase explanation: 1) pre-existing continental lithosphere stretches, and starts to break up; 2) continetal stretching and break-up continue, and lithosphere thins; 3) hyper-stretching, deep normal faults develop, continent finally breaks up, and underlying mantle exhumes; 4) seafloor spreading initiates, oceanic crustal accretes, but the beginning has poor magma amount; 5) seafloor spreading and oceanic crustal arrection continue, and magma supply progressively increases to normal.

5.2 Implications for Continental Break-up and Seafloor Spreading

From the MCS profile NH973-1 crossing SWSB, our

observations at its COB are in agreement with prior results about strong lithospheric extension evidenced by wide crustal thinning from tens of kilometers thick on the continent to several kilometers in the ocean, large seaward dipping faults as well as absence of seaward dipping reflectors in volcanic nature (Qiu *et al*., 2011; Lu *et al*., 2011; Ruan *et al*., 2011; Pichot *et al*., 2013; Ding *et al*., 2013; Yu *et al*., 2017). Continental break-up under this situation is usually hypothesized as non-volcanic margins (Skogseid, 2001; Menzies *et al*., 2002; Franke *et al*., 2013). Poor magma initiation and mantle exhumation may be attributed to this hypothesis. We observed nearly zero oceanic crust and two large low-angle normal faults at the south COB of SWSB (Fig.7), which match the signatures of magma-poor margin and exhumed upper mantle. To the north COB of the basin, unfortunately, we do not have MCS data to constrain whether it appears identically as the south. However, MCS profiles from the Phu Khanh Basin near the north margin of SWSB presented structures of strongly extended crust and consequent mantle exhumation (Savva *et al*., 2013). This adjacent basin may infer that SWSB may experience analogous continental stretching process.

Regarding SCS (Fig.1), the Northwest and East Subbasins (NWSB, ESB) show a few discrepancies from SWSB. MCS data over NWSB within the north margin of SCS show a narrow transition from thinning continental crust to normal oceanic crust, implying a very quick transition from continental break-up to seafloor spreading (Larsen *et al*., 2018). In addition, recent drilled basalts from the north COB of NWSB and ESB indicate vigorous magmatism at the initiation of seafloor spreading (Sun *et al*., 2018; Jian *et al*., 2018). These findings are contrary to our observations here about a wide crustal necking zone, little oceanic crust at COB, and possible mantle exhumation. It is interesting that within SCS three subbasins contain varied crustal structures on the rifted margins. The variations in SCS's COB structure styles seem to suggest that SWSB is different from NWSB and ESB in opening dynamics.

Furthermore, into the basin, oceanic crustal thicknesses of NWSB and ESB, are generally homogeneous as 7 km thick (McIntosh *et al*., 2014; Cameselle *et al*., 2015; Gao *et al*., 2015; Larsen *et al*., 2018). The constant thickness of the basin crust implies steady magma supply from the start to the end of seafloor spreading. Previously, similar to NWSB and ESB, SWSB was proposed to have normal oceanic crust based on seismic refraction modeling (*e.g*., Yao and Wang, 1983; Qiu *et al*., 2011). Here, in contrast, our results appear to contradict former arguments. SWSB shows variable crustal thickness, indicating that its oceanic crustal accretion varies with time during seafloor spreading (Fig.8). Notably, near the COB where the initial seafloor spreading happens, the crustal thickness of the basin is small (even zero), probably because of very limited magma supply at the beginning of seafloor spreading.

In comparison, processes of continental break-up and seafloor spreading occurred latest in SWSB relative to NWSB and ESB within SCS (Taylor and Hayes, 1980, 1983; Briais *et al*., 1993; Hsu *et al*., 2004; Barckhausen *et al*., 2014; Li *et al*., 2014). SWSB has the widest transition from continental break-up to oceanic crust at the rifted margins of SCS. The implication is that continental crust is hyper-stretched and tectonics is dominant in SWSB. SWSB produced thinnest oceanic crust and carried smallest amount of magma to start seafloor spreading, even though three sub-basins closed up at almost the same time (Li *et al*., 2014) and ended up with normal oceanic crustal thickness, *i.e*., nearly identical magma supply (Wu *et al*., 2012a; Zhang *et al*., 2016a; Ruan *et al*., 2016; Lu *et al*., 2016). Hence, magma supply is likely in steady state during seafloor spreading in NWSB and ESB, but varying in SWSB. Considering one single magmatic source for SCS, the supply to three sub-basins is not equal.

Structural and tectonic differences among the three sub-basins add complexity to the formation and evolution of SCS. The origin of SCS is often related to non-volcanic margin paradigms globally, like Iberia-Newfoundland margin (Boillot *et al*., 1995; Manatschal and Bernoulli, 1999; Whitmarsh *et al*., 2001; Hopper *et al*., 2007; Reston, 2007; Tucholke and Sibuet, 2007; Peron-Pinvidic and Manatschal, 2009), NW Australian margin (Karner and Driscoll, 1999), and Brazil-Angola margin (Mohriak *et al*., 1990; Contrucci *et al*., 2004; Aslanian *et al*., 2010; Contreras *et al*., 2010). In our study, SWSB appears to be a non-volcanic origin because of poor magmatism and strong tectonics as suggested by thin oceanic crust at the faulted COB. However, NWSB and ESB offer a distinct view of robust magmatism and rapid transition from continent to ocean (Sun *et al*., 2018; Jian *et al*., 2018; Larsen *et al*., 2018). All these imply that SWSB underwent different geodynamic processes in continental break-up and seafloor spreading from NWSB and ESB. SCS, commonly regarded as one tectonic unit, is supposed to have changes in creating its three sub-basins. Although crustal structure is not diagnostic of the proposed origin of SCS (extrusion-based or subduction-based or plume-induced models, *e.g*., Holloway, 1982; Briais *et al*., 1993; Hall, 2002; Replumaz and Tapponnier, 2003; Hall *et al*., 2008; Pubellier and Morley, 2014; Cullen *et al*., 2010; Xia *et al*., 2016), any mechanisms or their modifications/hybrids are required to explain the structural discrepancies among the three sub-basins within SCS.

6 Conclusions

Reprocessed MCS profile NH973-1 shows Moho structure across SWSB with unprecedented details, which help us to understand crustal formation and evolution of the basin and provides new insights to continental break-up and seafloor spreading processes of SCS. Main findings in this paper are summarized below:

The Moho of SWSB is generally symmetric on both sides of CRV in the middle of the basin.

Crustal thickness varies across SWSB. Beneath the oceanic crust in the basin center, the Moho is 2 s depth in TWTT (corresponding to 7 km), indicating normal oceanic crustal accretion during the ending of seafloor spreading.

Close to COB, the Moho becomes shallow to 1 s TWTT depth (3.5 km) under the igneous basement, implying strongly crustal thinning towards the continent, likely because of poor magma supply at the beginning of seafloor spreading. At south COB, the Moho depth is almost zero, *i.e*., nearly zero crustal thickness, which could be explained as a result of exhumed mantle.

Two large normal faults with low dipping angles were identified at south COB. The faults deeply penetrate the Moho into the upper mantle, which may have been caused by lithospheric hyper-stretching at COB during continental break-up.

Acknowledgements

We thank the scientists, crew, and technical staff of *R/V Tanbao* for collecting the seismic data. The research data used were provided by the National 973 Research Project of China and professor Pin Yan. We thank Xu Zhao for assistance in data processing and Yiming Luo for geographic plotting. This research was supported by the National Key R&D Program of China (No. 2018YFC03098 00), the National Natural Science Foundation of China (Nos. 91328205, 41376062, 91628301, U1606401, 4160 6 069, 41776058), the Natural Science Foundation of Guangdong Province in China (Nos. 2015A030310374, 2017A 030313243), the Chinese Academy of Sciences (Nos. Y4S L021001, QYZDY-SSW-DQC005) and the China Association of Marine Affairs (No. CAMAZD201714).

References

Aghaei, O., Nedimovic, M. R., Carton, H., Carbotte, S. M., Canales, J. P., and Mutter, J. C., 2014. Crustal thickness and Moho character of the fast-spreading East Pacific Rise from 9˚42´N to 9˚57´N from poststack-migrated 3D MCS data. *Geochemistry Geophysics Geosystems*, **15**: 634-657.

Aslanian, D., Moulin, M., Olivet, J. L., Unternehr, P., Matias, L., Bache, F., Rabineau, M., Nouze, H., Klingelheofer, F., Contrucci, I., and Labails, C., 2010. Brazilian and African passive margins of the central segment of the South Atlantic Ocean: Kinematic constraints. *Tectonophysics*, **468**: 98-112.

Barckhausen, U., Engels, M., Franke, D., Ladage, S., and Pubellier, M., 2014. Evolution of the South China Sea: Revised ages for breakup and seafloor spreading. *Marine and Petroleum Geology*, **58**: 599-611.

Boillot, G., Beslier, M. O., and Girardeau, J., 1995. *Nature, Structure and Evolution of the Ocean-Continent Boundary: The Lesson of the West Galicia Margin (Spain)*. Springer, Netherlands, 219-229.

Briais, A., Patrizt, P., and Tapponier, P., 1993. Updated interpretation of magnetic anomalies and seafloor spreading stages in the South China Sea: Implications for the tertiary tectonic of Southeast Asia. *Journal of Geophysical Research*, **98**: 6299-6328.

Cameselle, A. L., Ranero, C. R., Franke, D., and Barckhausen, U., 2015. The continent-ocean transition on the northwestern South China Sea. *Basin Research*, **29**: 1-23.

Contreras, J., Zuhlke, R., Bowman, S., and Bechstadt, T., 2010. Seismic stratigraphy and subsidence analysis of the southern Brazilian margin (Campos, Santos and Pelotas Basins). *Marine and Petroleum Geology*, **27**: 1952-1980.

Contrucci, I., Matias, L., Moulin, M., Geli, L., Klingelhofer, F., Nouze, H., Aslanian, D., Olivet, J. L., Rehault, J. P., and Sibuet, J. C., 2004. Deep structure of the West African continental margin (Congo, Zaire, Angola), between 5 degrees S and 8 degrees S, from reflection/refraction seismics andgravity data. *Geophysical Journal International*, **158**: 529-553.

Cullen, A., Reemst, P., Henstra, G., Gozzard, S., and Ray, A., 2010. Rifting of the South China Sea: New perspectives. *Petroleum Geoscience*, **16**: 273-282.

Ding, W., Franke, D., Li, J., and Steuer, S., 2013. Seismic stratigraphy and tectonic structure from a composite multi-channel seismic profile across the entire dangerous grounds, South China Sea. *Tectonophysics*, **582**: 162-176.

Ding, W., Li, J., Clift, P. D., and IODP Expedition 349 Scientists, 2016. Spreading dynamics and sedimentary process of the Southwest Sub-basin, South China Sea: Constraints from multichannel seismic data and IODP Expedition 349. *Journal of Asian Earth Sciences*, **115**: 97-113.

Dix, H. C., 1955. Seismic velocities from surface measurements. *Geophysics*, **20**: 68-86.

Franke, D., 2013. Rifting, lithosphere breakup and volcanism: Comparison of magma-poor and volcanic rifted margins. *Marine and Petroleum Geology*, **43**: 63-87.

Franke, D., Barckhausen, U., Baristeas, N., Engels, M., Ladage, S., Lutz, R., Montano, J., Pellejera, N., Ramos, E. G., and Schnabel, M., 2011. The continent-ocean transition at the southeastern margin of the South China Sea. *Marine and Petroleum Geology*, **28**: 1187-1204.

Franke, D., Savva, D., Pubellier, M., Steuer, S., Mouly, B., Auxietre, J., Meresse, F., and Chamot-Rooke, N., 2013. The final rifting evolution in the South China Sea. *Marine and Petroleum Geology*, **58**: 704-720.

Gao, J., Wu, S., McIntosh, K., Mi, L., Yao, B., Chen, Z., and Jia, L., 2015. The continent-ocean transition at the mid-northern margin of the South China Sea. *Tectonophysics*, **654**: 1-19.

Geoffroy, L., 2005. Volcanic passive margins. *Concise Review Geosciences*, **337**: 1395-1408.

Hall, R., 2002. Cenozoic geological and plate tectonic evolution of SE Asia and the SW Pacific: Computer-based reconstructions, model and animations. *Journal of Asian Earth Sciences*, **20**: 353-431.

Hall, R., van Hattum, M. W. A., and Spakman, W., 2008. Impact of India-Asia collision on SE Asia: The record in Borneo. *Tectonophysics*, **451**: 366-369.

Holbrook, W. S., Reiter, E. C., Purday, G. M., and Toksoz, M. N., 1992. Image of the Moho across the continent-ocean transition, United States east-coast. *Geology*, **20**: 203-206.

Holloway, N. H., 1982. North Palawan Block, Philippines – Its relation to Asian Mainland and role in the evolution of South China Sea. *American Association of Petroleum Geologists Bulletin*, **66**: 1355-1383.

Hopper, J. R., Funck, T., and Tucholke, B. E., 2007. Structure of the Flemish Cap margin, Newfoundland: Insights into mantle and crustal processes during continental breakup. In: *Imaging, Mapping, and Modelling Continental Lithosphere Extension and Breakup*. Karner, G. D., *et al*., eds., Geological Society of Lodon Special Publications, London, 47-61.

Hsu, S. K., Yeh, Y. C., Doo, W. B., and Tsai, C. H., 2004. New bathymetry and magnetic lineations identifications in the northernmost South China Sea and their tectonic implications. *Marine Geophysical Research*, **25**: 29-44.

Hu, D., Zhou, D., Wu, X., He, M., Pang, X., and Wang, Y., 2009. Crustal structure and extension from slope to deepsea basin in

the northern South China Sea. *Journal of Earth Science*, **20**: 27-37.

Jian, Z., Larson, H. C., Zarikian, C. A., and the Expedition 368 Scientists, 2018. *Expedition 368 Preliminary Report: South China Sea Rifted Margin*. International Ocean Discovery Program, Texas, 1-54.

Karner, G. D., and Driscoll, N. W., 1999. Style, timing and distribution of tectonic deformation across the Exmouth Plateau, northwest Australia, determined from stratal architecture and quantitative basin modelling. *Geological Society of London Special Publicatiions*, **164**: 271-311.

Kearey, P., Klepeis, K. A., and Vine, F. J., 2009. *Global Tectonics*. Third edition. Wiley-blackwell, United Kingdom, 1-482.

Kent, G. M., Harding, A. J., Orcutt, J. A., Detrick, R. S., Mutter, J. C., and Buhl, P., 1994. Uniform accretion of oceanic crust south of the Garrett transform at 14°42′S on the East Pacific Rise. *Journal of Geophysical Research*, **99**: 9097-9116.

Korenaga, J., and Sager, W. W., 2012. Seismic tomography of Shatsky Rise by adaptive importance sampling. *Journal of Geophysical Research*, **117**: 70-83.

Larsen, H. C., Mohn, G., Nirrengarten, M., and the Expeditions 367/368 Scientists, 2018. Rapid transition from continental breakup to oceanic crust at South China Sea rifted margin. *Nature Geoscience*, **11**: 782-789.

Lei, C., and Ren, J., 2016. Hyper-extended rift systems in the Xisha Trough: Implications for extreme crustal thinning ahead of a propagating ocean of the South China Sea. *Marine and Petroleum Geology*, **77**: 846-864.

Lei, C., Ren, J., Pang, X., Chao, P., and Han, X., 2018. Continental rifting and sediment infill in the distal part of the northern South China Sea in the Western Pacific region: Challenge on the present-day models for the passive margins. *Marine and Petroleum Geology*, **93**: 166-181.

Li, C. F., Xu, X., Lin, J., Sun, Z., Zhu, J., Yao, Y., Zhao, X., Liu, Q., Kulhanek, D. K., Wang, J., Song, T., Zhao, J., Qiu, N., Guan, Y., Zhou, Z., Williams T., and IODP 349 shipboard scientists, 2014. Ages and magnetic structures of the South China Sea constrained by deep tow magnetic surveys and IODP Expedition 349. *Geochemistry Geophysics Geosystems*, **15**: 4958-4983.

Li, J., 2011. Dynamics of the continental margins of South China Sea: Scientific experiments and research progresses. *Chinese Journal of Geophysics*, **54**: 2993-3003 (in Chinese with English abstract).

Li, J., Ding, W., Wu, Z., Zhang, J., and Dong, C., 2012. The propagation of seafloor spreading in the southwestern subbasin, South China Sea. *Chinese Science Bulletin*, **57**: 1896-1905 (in Chinese with English abstract).

Lu, C., Hao, T., Lin, J., and Qiu, X., 2016. The role of rifting in the development of the continental margins of the southwest subbasin, South China Sea: Insights from an OBS experiment. *Marine Geophysical Research*, **38**: 1-19.

Lu, C., Hao, T., Qiu, X., Zhao, M., and You, Q., 2011. A study on the deep structure of the northern part of southwest subbasin from ocean bottom seismic data, South China Sea. *Chinese Journal of Geophysics*, **54**: 3129-3138 (in Chinese with English abstract).

Manatschal, G., and Bernoulli, D., 1999. Architecture and tectonic evolution of nonvolcanic margins: Present-day Galicia and ancient Adria. *Tectonics*, **18**: 1099-1119.

McIntosh, K., Lavier, L., Van Avendonk, H., Lester, R., Eakin, D., and Liu, C., 2014. Crustal structure and inferred rifting processes in the northwest South China Sea. *Marine and Petroleum Geology*, **58**: 612-626.

Menzies, M. A., Klemperer, S. L., Ebinger, C. J., and Baker, J., 2002. Characteristics of volcanic rifted margins. *Special Paper of the Geological Society of America*, **362**: 1-14.

Mohriak, W. U., Mello, M. R., Dewey, J. F., Maxwell, J. R., 1990. Petroleum geology of the Campos Basin, offshore Brazil. *Geological Society London Special Publications*, **50**: 119-141.

Mutter, J. C., and Carton, H. D., 2013. The Mohorovicic discontinuity in ocean basins: Some observations from seismic data. *Tectonophysics*, **609**: 314-330.

Nedimovic, M. R., Carbotte, S. M., Harding, A. J., Detrick, R. S., Canales, J. P., Diebold, J. B., Kent, G. M., Tischer, M., and Babcock, J. M., 2005. Frozen magma lenses below the oceanic crust. *Nature*, **436**: 1149-1152.

Peron-Pinvidic, G., and Manatschal, G., 2009. The final rifting evolution at deep magma-poor passive margins from Iberia-Newfoundland: A new point of view. *International Journal of Earth Sciences*, **98**: 1581-1597.

Pichot, T., Delescluse, M., Chamot-Rooke, N., Pubellier, M., Qiu, Y., Meresse, F., Sun, G., Savva, D., Wong, K. P., Watremez, L., and Auxietre, J. L., 2013. Deep crustal structure of the conjugate margins of the SW South China Sea from wide-angle refraction seismic data. *Marine and Petroleum Geology*, **58**: 627-643.

Prada, M., Sallares, V., Ranero, C. R., Guzman, M., Zitellini, N., Grevemeyer, I., de Franco, R., and Medoc Cruise Party, 2012. Deep structure of the Tyrrhenian Basin from 2-D joint refraction and reflection travel-time tomography of wide angle seismic data. *EGU General Assembly 2012*. Vienna, Austria, 10323.

Pubellier, M., and Morley, C. K., 2014. The basins of Sundaland (SE Asia): Evolution and boundary conditions. *Marine and Petroleum Geology*, **58**: 555-578.

Qiu, X., Zhao, M., Ao, W., Lu, C., Hao, T., You, Q., Ruan, A., and Li, J., 2011. OBS survey and crustal structure of the Southwest Sub-basin and Nansha Block, South China Sea. *Chinese Journal of Geophysics*, **54**: 3117-3128 (in Chinese with English abstract).

Replumaz, A., and Tapponnier, P., 2003. Reconstruction of the deformed collision zone between India and Asia by backward motion of lithospheric blocks. *Journal of Geophysical Research*, **108**: 2285-2309.

Reston, T., 2007. Extension discrepancy at North Atlantic non-volcanic rifted margins: Depth-dependent stretching or unrecognized faulting? *Geology*, **35**: 367-370.

Rohr, K. M. M., Milkereit, B., and Yorath, C. J., 1988. Asymmetric deep crustal structure across the Juan de Fuca Ridge. *Geology*, **16**: 533-537.

Ruan, A., Niu, X., Qiu, X., Li, J., Wu, Z., Zhao, M., and Wei, X., 2011. A wide angle ocean bottom seismometer profile across Liyue Bank, the southern margin of South China Sea. *Chinese Journal of Geophysics*, **54**: 3139-3149 (in Chinese with English abstract).

Ruan, A., Wei, X., Niu, X., Zhang, J., Dong, C., Wu, Z., and Wang, X., 2016. Crustal structure and fracture zone in the central basin of the South China Sea from wide angle seismic experiments using OBS. *Tectonophysics*, **688**: 1-10.

Sandwell, D. T., and MacKenzie, K. R., 1989. Geoid height versus topography for oceanic plateaus and swells. *Journal of Geophysical Research*, **94**: 7403-7418.

Sandwell, D. T., and Smith, W. H. F., 1997. Marine gravity anomaly from Geosat and ERS-1 satellite altimetry. *Journal of Geophysical Research*, **102**: 10039-10054.

Savva, D., Meresse, F., Pubellier, M., Chamot-Rooke, N., Lavier,

L., Wong, P. K., Franke, D., Steuer, S., Sapin, F., Auxietre, J. L., and Lamy, G., 2013. Seismic evidence of hyper-stretched crust and mantle exhumation offshore Vietnam. *Tectonophysics*, **608**: 72-83.

Skogseid, J., 2001. Volcanic margins: Geodynamic and exploration aspects. *Marine and Petroleum Geology*, **18**: 457-461.

Smith, W. H. F., and Sandwell, D. T., 1997. Global seafloor topography from satellite altimetry and ship depth soundings. *Science*, **277**: 1957-1962.

Song, T., and Li, C., 2015. Rifting to drifting transition of the southwest subbasin of the South China Sea. *Marine Geophysical Research*, **36**: 167-185.

Steinhart, J. S., 1967. Mohorovicic discontinuity. In: *International Dictionary of Geophysics, Volume 2*. Runcorn, S. K., ed., Pergamon Press, Oxford, 991-994.

Sun, Z., Stock, J., Klaus, A., and the Expedition 367 Scientists, 2018. *Expedition 367 Preliminary Report: South China Sea Rifted Margin*. International Ocean Discovery Program, Texas, 1-33.

Taylor, B., and Hayes, D. E., 1980. The tectonic evolution of the South China Sea Basin. In: *The Tectonic and Geologic Evolution of Southeast Asian Seas and Islands*. Hayes, D. E., ed., American Geophysical Union Geophysical Monograph, Washington, D. C., 89-104.

Taylor, B., and Hayes, D. E., 1983. Origin and history of the South China Sea Basin. In: *The Tectonic and Geologic Evolution of Southeast Asian Seas and Islands: Part 2*. Hayes, D. E., ed., American Geophysical Union Geophysical Monograph, Washington, D. C., 23-56.

Tucholke, B. E., and Sibuet, J. C., 2007. Leg 210 synthesis: Tectonic, magmatic, and sedimentary evolution of the Newfoundland-Iberia Rift. *Proceedings of the Ocean Drilling Program Scientific Results 210*, 1-56.

Wang, Y., Qiu, Y., Yan, P., Zheng, H., Liu, H., and Wang, J., 2016. Seismic evidence for Mesozoic strata in the northern Nansha waters, South China Sea. *Tectonophysics*, **677**: 190-198.

Whitmarsh, R. B., Minshull, T. A., Russell, S. M., Dean, S. M., Louden, K. E., and Chian, D., 2001. The role of syn-rift magmatism in the rift-to-drift evolution of the West Iberia continental margin: Geophysical observations. *Geological Society London Special Publications*, **187**: 107-124.

Wu, Z., Li, J., Ruan, A., Lou, H., Ding, W., Niu, X., and Li, X., 2012a. Curstal structure of the Northwestern Sub-basin, South China Sea: Results from a wide-angle seismic experiment. *Science China–Earth Sciences*, **55**: 159-172.

Wu, Z., Ruan, A., Li, J., Li, S., Qiu, X., and Ding, W., 2012b. Wide-angle seismic exploration in the Southwest Sub-basin of the South China Sea. *Journal of Tropical Oceanography*, **31**: 35-39 (in Chinese with English abstract).

Xia, S., Zhao, D., Sun, J., and Huang, H., 2016. Teleseismic imaging of the mantle beneath southernmost China: New insights into the Hainan plume. *Gondwana Research*, **36**: 46-56.

Yan, P., Deng, H., Liu, H., Zhang, Z., and Jiang, Y., 2006. The temporal and spatial distribution of volcanism in the South China Sea region. *Journal of Asian Earth Science*, **27**: 647-659.

Yao, B., and Wang, G., 1983. Crustal structure of South China Sea Basin. *Science China*, **2**: 177-186 (in Chinese with English abstract).

Yu, Z., Li, J., Ding, W., Zhang, J., Ruan, A., and Niu, X., 2017. Crustal structure of the southwest subbasin, South China Sea, from wide-angle seismic tomography and seismic reflection imaging. *Marine Geophysical Research*, **38**: 85-104.

Zhang, J., Li, J., Ruan, A., Wu, Z., Yu, Z., Niu, X., and Ding, W., 2016a. The velocity structure of a fossil spreading centre in the Southwest Sub-basin, South China Sea. *Geological Journal*, **51**: 548-561.

Zhang, J., Sager, W. W., and Korenaga, J., 2016b. The seismic Moho structure of Shatsky Rise oceanic plateau, northwest Pacific Ocean. *Earth Planetary Science Letters*, **441**: 143-154.

Zhao, C., Song, H., Li, J., Song, Y., and Tian, L., 2011. Tectonic and seismic interpretation of line NH973-1 along Southwest Sub-basin in South China Sea. *Chinese Journal of Geophysics*, **54**: 3258-3268 (in Chinese with English abstract).

(Edited by Chen Wenwen)